Effect of Zr on the crystallographic texture of precipitation-hardened $Sm(Co,Fe,Cu,Zr)_7$ ribbons

Chuan-bing Rong,[a] Hong-wei Zhang, Shu-li He, Ren-jie Chen, and Bao-gen Shen
State Key Laboratory of Magnetism, Institute of Physics and Centre for Condensed Matter Physics, Chinese Academy of Sciences, People's Republic of Beijing 100080, China

(Received 1 November 2004; accepted 21 February 2005; published online 15 March 2005)

$Sm(Co_{bal}Fe_{0.1}Cu_{0.1}Zr_w)_7$ ($w=0.01-0.09$) ribbons have been prepared by conventional melt spinning followed by precipitation hardening. The Zr addition can suppress the nucleation of solidification and increase the velocity of grain growth. This leads to the increase of texture degree of the ribbons with increasing Zr content. The crystallographic texture is still preserved in ribbons after the precipitation hardening. The remanence ratio of the heat-treated ribbons increases from 0.7 for $w=0.01$ to 0.9 for $w=0.08$. An energy product of about 10 MGOe has been obtained in the ribbon with $w=0.03$. The angular dependence of coercivity suggests that the magnetization reversal of the precipitation-hardened ribbons is controlled by both domain-wall pinning and nucleation mechanism. © *2005 American Institute of Physics*. [DOI: 10.1063/1.1888038]

The $Sm(Co,Fe,Cu,Zr)_z$ sintered magnets exhibit outstanding thermal stability and high energy products $(BH)_{max}$ at elevated temperatures due to their high Curie temperatures and large anisotropy fields.[1–3] It is generally accepted that the high coercivity H_c in these precipitation-hardened magnets results from the coexistence of a cellular microstructure with rhombohedral 2:17 cells surrounded by hexagonal 1:5 cell boundaries. A Zr-rich lamellar phase is superimposed on the cellular microstructure. However, the complex microstructure is usually obtained after a lengthy heat treatment consisting of homogenization at high temperatures followed by aging at temperatures in the range of 800–850 °C and slow cooling to 400 °C. Therefore, some efforts have been undertaken to simplify the above processing procedure.[4,5] Unfortunately, $Sm(Co,Fe,Cu,Zr)_z$ magnets obtained through the simple process are always isotropic. As a result, their $(BH)_{max}$ is far lower than those of the anisotropic $Sm(Co,Fe,Cu,Zr)_z$ magnets prepared by the traditional powder metallurgical sintering route or bonding technique.[2,6]

Recently, it has been found that the anisotropic magnets can be obtained by a melt-spinning technique at low wheel velocities.[7–9] A preference for *c*-axis orientation normal to or parallel to the surface of melt-spun ribbons has been observed in RE–Fe–B[7,8] and Sm–Co[9] systems, respectively. However, anisotropic precipitation-hardened $SmCo_5$/Sm_2Co_{17} ribbons have not been obtained up to now. Numerous investigations show that the metastable 1:7 phase could be segregated into a mixture of 2:17 and 1:5 phases by precipitation hardening in recent years.[10,11] Since the grain-boundary and cellular phases are coherent, the anisotropic $Sm(Co,Fe,Cu,Zr)_z$ magnets may be obtained easily if the anisotropic 1:7-type ribbons can be prepared by melt spinning. In this letter, the $TbCu_7$-type $Sm(Co_{bal}Fe_{0.1}Cu_{0.1}Zr_w)_7$ ribbons were prepared by melt spinning. It was found that the degree of texture of the ribbons increased with increasing Zr content. The crystallographic texture was still preserved after the precipitation hardening. Remanence ratio about 0.9 and energy product about 10 MGOe were obtained in the precipitation-hardened ribbons with $w=0.08$ and 0.03, respectively.

Ingots with nominal composition $Sm(Co_{bal}Fe_{0.1}Cu_{0.1}Zr_w)_7$ with $x=0.01-0.09$ were prepared by arc-melting technique. The ribbons were obtained using the single-roller melt spinning technique with the surface speeds of the Cu wheel about 5 m/s. Subsequently, they were isothermally aged at 850 °C for 3 h followed by slow cooling at 1 °C/min to 400 °C and then quenched to room temperature. Crystalline structure was determined by x-ray diffraction (XRD) with Cu $K\alpha$ radiation. Scanning electron micrographs (SEM) were used to show microstructure of the samples. The magnetic measurements were performed using a superconducting quantum interference device magnetometer and a vibrating sample magnetometer.

Figures 1(a) and 1(b) display the typical XRD patterns of melt-spun and precipitation-hardened $Sm(Co_{bal}Fe_{0.1}Cu_{0.1}Zr_w)_7$ ribbons, respectively. As can be seen from Fig. 1(a), the as-spun ribbons mainly consist of a single $TbCu_7$-type phase. This means that the solid solution

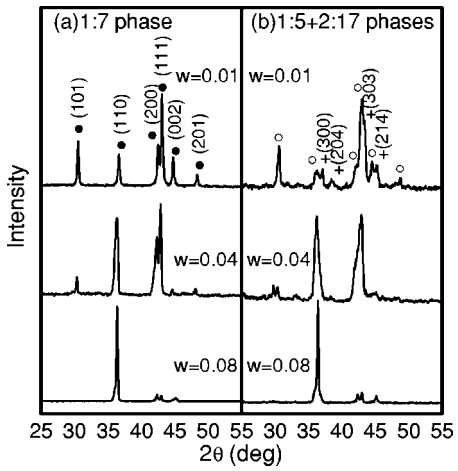

FIG. 1. Typical XRD patterns of (a) melt-spun and (b) precipitation-hardened $Sm(Co_{bal}Fe_{0.1}Cu_{0.1}Zr_w)_7$ ribbons, respectively. Diffraction peaks marked with (●), (○) and (+) belong to the 1:7, 1:5, and 2:17 phases, respectively.

[a]Author to whom correspondence should be addressed; electronic mail: rongcb@g203.iphy.ac.cn

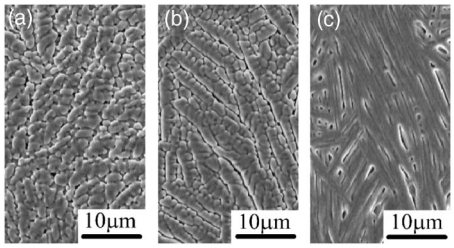

FIG. 2. SEM images taken from the free surface of melt-spun $Sm(Co_{bal}Fe_{0.1}Cu_{0.1}Zr_w)_7$ ribbons. (a) $z=0.01$, (b) $z=0.04$, and (c) $z=0.08$.

treatment, which is required for the bulk precipitation-hardened magnets, is not necessary for the melt-spun materials. No obviously preferential orientation of the crystallites is observed from the diffraction peaks of the sample with $w=0.01$. However, the enhanced intensity of the (110) peak for the sample with $w=0.04$ suggests that the partially preferential orientation is obtained. Further Zr substitution leads to a more pronounced increase in the intensity of (110) peak and the crystallographic texture is obtained in the ribbon with $w=0.08$. The c axis of crystallites is supposed to lie in plane.

As shown in Fig. 1(b), the 1:7 phase of the melt-spun ribbons is segregated into 1:5 and 2:17 phases after precipitation hardening. In particular, the (204) peak is characteristic of the 2:17 phase but absent in the 1:5 and 1:7 phases. The broadened peaks of the precipitation-hardened samples indicate that the phase transformation leads to the formation of a fine microstructure. This is similar to that observed in Refs. 11–14. More interesting, the XRD patterns of the annealed ribbons are very similar to those of the melt-spun ribbons. This means that the crystallographic texture is still preserved in ribbons after precipitation hardening.

The previous studies show that solidification starts at the surface in contact with the wheel in the case of single-roller quenching.[7,8] The large temperature gradient between the wheel surface and the nozzle of the quartz tube always causes the formation of dendrite structure, which is observed in SEM micrographs taken from the cross section of all ribbons. However, the Zr substitution results in a significant modification to the microstructure of the ribbon surface. Figure 2 presents the SEM micrographs of the free-side surface of the as-spun ribbons with different Zr content. The small grains of approximately 1 μm in diameter are obtained in the ribbon with $w=0.01$. No obvious preferential grain growth is observed in this low Zr content ribbon. Whereas, the columnar dendrite grains, with their long axes mainly parallel to the longitudinal axes of the ribbons, is formed in the ribbon with $w=0.04$. The average grain size is about 2 μm $\times 15$ μm. With further Zr substitution, it can be found clearly that the columnar dendrite grains arrange more formally and compactly than those of low Zr content ribbons. It is supposed that the Zr addition favors the formation of preferential orientation, which agrees closely with the XRD analyses.

It is well known that the solidification process is composed of two steps: Nucleation and growth. The previous studies show that the addition of Cu to the Fe–Si–B[15] or Sm–Fe–Si–C[16] alloys increases the nucleation rate and limits the grain growth and thus leads to the formation of fine grain size. In this work, the presence of Cu may also result in the formation of the small grain sizes in the ribbon with $w=0.01$. However, the large and compact columnar dendrite grains of the ribbon with $w=0.08$ means that the addition of Zr can suppress the nucleation of solidification and increase the velocity of grain growth. This is the reason that the crystalline texture is formed in the high Zr content ribbons. A moderate case is presented in Fig. 2(b). Although the microstructure of the ribbon with $w=0.04$ also consists of large columnar dendrite grain, each dendrite grain is composed of several small grains.

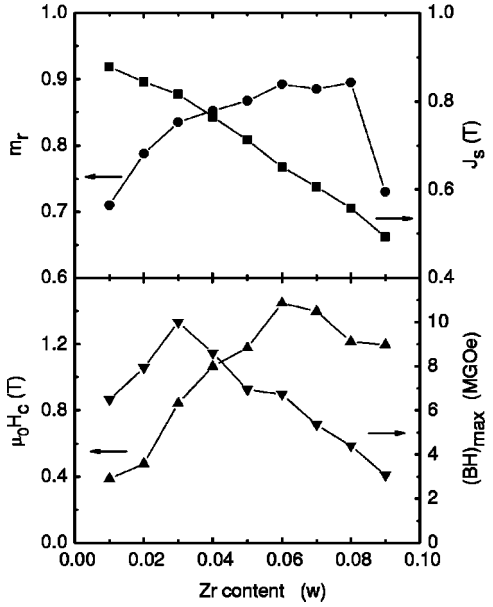

FIG. 3. Variations of m_r, J_s, H_c and $(BH)_{max}$ as a function of Zr content for the precipitation-hardened $Sm(Co_{bal}Fe_{0.1}Cu_{0.1}Zr_w)_7$ ribbons.

Figure 3 shows the magnetic properties of the precipitation-hardened $Sm(Co_{bal}Fe_{0.1}Cu_{0.1}Zr_w)_7$ ribbons as a function of Zr content. It is found that remanence ratio $m_r=J_r/J_s$, where J_r and J_s are remanence and saturation magnetization, respectively, increases from 0.7 for $w=0.01$ to 0.9 for $w=0.08$. Further Zr substitution leads to the sharp drop of m_r. The m_r vs w plot can be attributed to the variation of the texture degree of the ribbons with the Zr addition. H_c increases markedly with increasing w and reaches the maximum of 1.5 T at $w=0.06$ due to the increases of the amount of Zr-rich lamellar phase.[3] Unfortunately, the addition of Zr lowers J_s of the ribbons since J_s of the Zr-rich phase is far lower than that of 1:5 or 2:17 phases.[10] $(BH)_{max}$ increases initially due to the improvement of rectangularity of the demagnetization curves. It reaches a maximum value of about 10 MGOe at $w=0.03$, and then falls off due to the fast drop of J_s.

The dependence of $H_c(\theta)$ as a function of the angle θ between the applied field and the easy axis can be used as a probe of the magnetization reversal mechanism. The resistance against domain-wall displacement should lead to a coercivity law of the type $1/\cos\theta$.[17] The $1/\cos\theta$ law is often associated with the pinning mechanism. If the reversal mechanism is coherent rotation, the angular dependence should follow the Stoner–Wohlfarth (SW) law.[18] H_c is equal to $1/[(\cos\theta)^{2/3}+(\sin\theta)^{2/3}]^{3/2}$ for $0\leqslant\theta\leqslant\pi/4$ and $\sin(2\theta)/2$ for $\pi/4\leqslant\theta\leqslant\pi/2$. The existence of coherent rotation is an indication of nucleation, because in this case the magnetic reversal occurs without domain-wall displacement. Figure 4 gives the angular dependence of coercivity for the sample

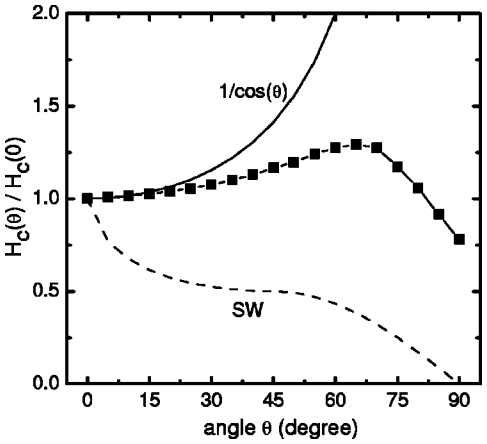

FIG. 4. Angular coercivity dependence for the sample with $w=0.08$. The Stoner–Wohlfarth (SW) law and the $1/\cos\theta$ law are also plotted.

with $w=0.08$. As can be observed in Fig. 4, the angular dependence of coercivity suggests that the magnetization reversal of the sample is controlled by both domain-wall pinning and nucleation mechanism. This result is in agreement with previous proposals.[19]

In summary, anisotropic $TbCu_7$-type $Sm(Co_{bal}Fe_{0.1}Cu_{0.1}Zr_w)_7$ ribbons have been prepared by melt spinning at a low wheel velocity. The Zr addition can suppress the nucleation solidification and increase the velocity of grain growth. This leads to the increase of texture degree of the ribbons with increasing Zr content. The crystallographic texture is preserved after precipitation hardening. A maximum m_r about 0.9 and $(BH)_{max}$ about 10 MGOe have been obtained in the ribbons with $w=0.08$ and 0.03, respectively. The magnetization reversal of the precipitation-hardened ribbons is controlled by both domain-wall pinning and nucleation mechanism.

The work was supported by the State Key Project of Fundamental Research and the National Science Foundation of China.

[1]A. E. Ray and S. Liu, J. Mater. Eng. Perform. **1**, 183 (1992).
[2]C. H. Chen, M. S. Walmer, M. H. Walmer, S. Liu, E. Kuhl, and G. Simon, J. Appl. Phys. **83**, 6706 (1998).
[3]G. C. Hadjipanayis, W. Tang, Y. Zhang, S. T. Chui, J. F. Liu, C. Chen, and H. Kronmuller, IEEE Trans. Magn. **36**, 3382 (2000).
[4]W. Tang, Y. Zhang, and G. C. Hadjipanayis, Appl. Phys. Lett. **77**, 421 (2000).
[5]A. Yan, A. Bollero, K. H. Muller, and O. Gutfleisch, Appl. Phys. Lett. **80**, 1243 (2002).
[6]B. M. Ma, W. Gong, C. O. Bounds, C. H. Chen, and M. S. Walmer, J. Appl. Phys. **83**, 6712 (1998).
[7]D. Dadon, Y. Gefen, and M. P. Dariel, IEEE Trans. Magn. **23**, 3605 (1987).
[8]T. Fuji, R. C. O'Handley, and N. J. Grant, Appl. Phys. Lett. **54**, 2487 (1989).
[9]A. Yan, W. Y. Zhang, H. W. Zhang, and B. G. Shen, J. Appl. Phys. **88**, 2787 (2000).
[10]Y. Fukui, T. Nishio, and Y. Iwama, IEEE Trans. Magn. **23**, 2705 (1987).
[11]J. Zhou, R. Skomski, C. Chen, G. C. Hadjipanayis, and D. J. Sellmyer, Appl. Phys. Lett. **77**, 1514 (2000).
[12]W. Tang, Y. Zhang, and G. C. Hadjipanayis, J. Appl. Phys. **91**, 7896 (2002).
[13]J. Zhang, H. Liu, C. B. Rong, H. W. Zhang, S. Y. Zhang, B. G. Shen, Y. Q. Bai, and B. H. Li, Appl. Phys. Lett. **83**, 1172 (2003).
[14]C. B. Rong, H. W. Zhang, J. Zhang, X. B. Du, S. Y. Zhang, and B. G. Shen, J. Appl. Phys. **97**, 33907 (2005).
[15]Y. Yoshizawa, S. Oguma, and K. Yamauchi, J. Appl. Phys. **64**, 6044 (1988).
[16]H. W. Zhang, S. Y. Zhang, B. G. Shen, and F. W. Wang, J. Magn. Magn. Mater. **187**, 247 (1998).
[17]H. Kronmuller, K. D. Durst, and G. Martinek, J. Magn. Magn. Mater. **149**, 69 (1987).
[18]E. C. Stoner and E. P. Wohlfarth, Philos. Trans. R. Soc. London, Ser. A **240**, 599 (1948).
[19]M. M. Corte-Real, M. F. de Campos, Y. Zhang, G. C. Hadjipanayis, and J. F. Liu, Phys. Status Solidi A **193**, 302 (2002).